CHALMERS
UNIVERSITY OF TECHNOLOGY

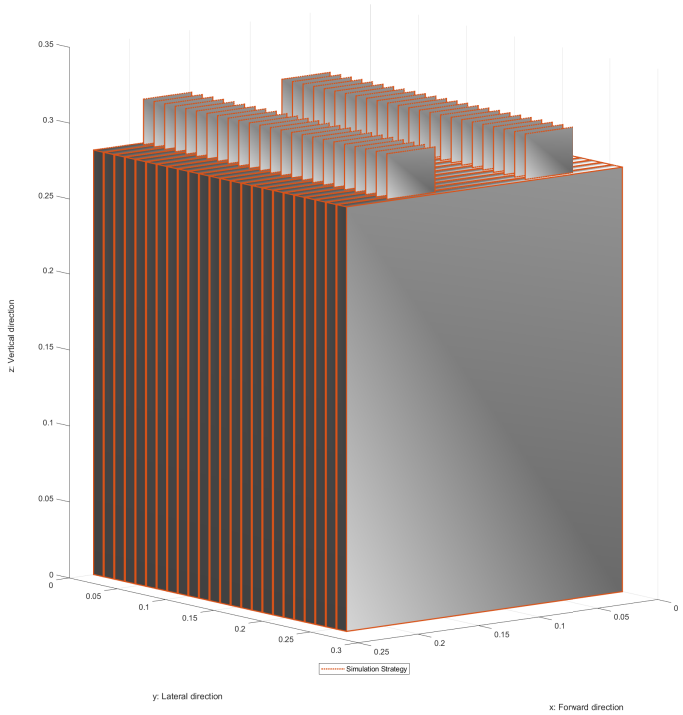

Enhancing EV Battery Recycling Through Discharge Optimization

Implementation of Prediction-Based Control Strategies to Streamline Battery Discharge and Ensure Safe Temperature Levels

Master's thesis in Systems, Control and Mechatronics

ADAM BURMAN

DEPARTMENT OF ELECTRICAL ENGINEERING

CHALMERS UNIVERSITY OF TECHNOLOGY
Gothenburg, Sweden 2024
www.chalmers.se

Master's thesis 2024

Enhancing EV Battery Recycling Through Discharge Optimization

Implementation of Prediction-Based Control Strategies to Streamline Battery Discharge and Ensure Safe Temperature Levels

ADAM BURMAN

CHALMERS
UNIVERSITY OF TECHNOLOGY

Department of Electrical Engineering
Systems, Control and Mechatronics
Automatic Control
Chalmers University of Technology
Gothenburg, Sweden 2024

Enhancing EV Battery Recycling Through Discharge Optimization
Implementation of Prediction-Based Control Strategies to Streamline Battery Discharge and Ensure Safe Temperature Levels
ADAM BURMAN

Supervisors: Changfu Zou, Associate Professor at Automatic Control
Meng Yuan, Postdoc at Automatic Control
Examiner: Changfu Zou

Master's Thesis 2024
Department of Electrical Engineering
Systems, Control and Mechatronics
Automatic Control
Chalmers University of Technology
SE-412 96 Gothenburg
Telephone +46 31 772 1000

Cover: An illustration of a 12s2p battery module model, along with its thermal simulation strategy, created by the author using MATLAB's Battery Builder toolbox.

Typeset in LaTeX
Printed by Chalmers Reproservice
Gothenburg, Sweden 2024

Enhancing EV Battery Recycling Through Discharge Optimization
ADAM BURMAN
Department of Electrical Engineering
Chalmers University of Technology

Abstract

The use of lithium-ion (Li-ion) batteries for electric vehicles (EVs) has increased exponentially and is expected to continue growing with the electrification of transportation. The increased usage of Li-ion batteries poses new challenges for reusing materials and improving the efficiency of battery recycling. Battery modules from electric vehicles that have reached their end of life (EOL) are fully discharged prior to recycling and minimizing discharge time is crucial for the industry. This study evaluates discharge current profiles generated by control strategies based on discharge time and the ability to maintain a safe internal battery temperature. The evaluation is performed using Simulink models of a table-based battery cell and a battery module representing a module in a 12s2p configuration based on the LG Chem E78 battery pouch cell. The controllers tested include constant current constant voltage (CC-CV), constant current constant temperature (CC-CT), dynamic programming (DP), and robust model predictive control (MPC). The results indicate that to avoid violating temperature constraints, controllers using model-based prediction and incorporating real-time measurement data with a Kalman filter, such as robust MPC, achieve the shortest discharge time without violating temperature constraints, showing promise for future applications.

Keywords: Discharge Time Optimization, Temperature Constraint, Robust Model Predictive Control (MPC), Proportional-Integral (PI) Control, Battery Modeling.

Acknowledgements

I would like to express my gratitude to my supervisors Changfu Zou and Meng Yuan for sharing their expertise in control and battery systems, allowing me to complete my master's studies with a project relevant both today and in the future of battery recycling.

My sincere thanks also go to the battery research group for their time, insights, and willingness to discuss my many questions.

Finally, my heartfelt thanks go to Sonja, for her endless patience and understanding during the many late-night coding sessions, including countless "just one more simulation" promises - even when leaving for Italy. And to my mother, Pia, who may not fully understand what I do, but has listened to me talk about it more than anyone ever should. Their support has been my constant in this journey.

Thank you.

Adam Burman, Gothenburg, November 2024

List of Acronyms

Below is the list of acronyms that have been used throughout this thesis, listed in alphabetical order:

CC-CV	Constant current constant voltage
CC-CT	Constant current constant temperature
DP	Dynamic programming
ECM	Equivalent circuit model
EOL	End-of-life
ESC	External short-circuit
EV	Electric vehicle
Li-ion	Lithium-ion
LIB	Lithium-ion battery
LQR	Linear-quadratic regulator
MPC	Model predictive control
OCV	Open-circuit voltage
PI	Proportional-integral controller
RC	Resistor-capacitor
SoC	State of charge
SoE	State of energy
SoH	State of health

Nomenclature

Below is the nomenclature of indices, sets, parameters, and variables that have been used throughout this thesis.

Indices

i,j	Indices (multiple use-cases)
t	Index for continuous time
k	Index for discrete time

Parameters

12s2p	Configuration of cells in a module, 2 parallel lines of 12 cells in series
A	State matrix
A_{cl}	Closed-loop state matrix
B	Input matrix
C_1	Capacitance in RC pair
C_A	Available capacity
C_c	Core heat capacity
C_N	Nominal capacity
C_s	Surface heat capacity
d_i	Disturbance impact
d_{db}	Disturbance bound
E_{nom}	Nominal energy
K_{LQR}	Optimal feedback gain matrix
n_x	Number of states
N	Prediction horizon (MPC) or No. of variables (DP)

$\{p_i\}_{i=1}^{5}$	Polynomial coefficients for OCV-SOC estimation
Q_u	Input penalty matrix
Q_x	State penalty matrix
Q_{LQR}	State cost matrix for LQR
R_0	Internal resistance
R_1	Resistance in RC pair
R_c	Conduction resistance
R_u	Convection resistance
R_{LQR}	Input cost matrix for LQR
t_f	Final time for complete discharge
t_h	Hold time for zero-order hold
t_s	Sampling time
T_c	Core temperature
T_s	Surface temperature
$\mathcal{J}$	Cost function
$\mathcal{J}_N$	Terminal penalty
η	Energy efficiency of battery
$\mathbf{x}_0$	Initial condition

Variables

I	Current
V_1	Voltage over RC pair
V_T	Terminal voltage
$\mathbf{x}$	States
$\mathbf{x}_{\text{op}}$	State operating point for linearization
$\mathbf{u}_{\text{op}}$	Input operating point for linearization
$\mathbf{u}$	Inputs
$\tilde{\mathbf{x}}$	State setpoint
$\tilde{\mathbf{u}}$	Input setpoint

Contents

List of Figures

List of Tables

1
Introduction

The rapid proliferation of EVs has led to a significant increase in demand for batteries. The global demand for Li-ion batteries increased by about 65% to 550 GWh between 2021 and 2022 and some projections expect a continued demand up to 2000 GWh by the year 2030. The increased demand implies a growing increase in the interest not only in the production of Li-ion batteries but also maximizing the lifetime and potential of each battery produced[1].

First Life - During the primary service life of an EV battery, the battery is subjected to various operating conditions, charge and discharge cycles, aging, and thermal stress. These factors contribute to the degradation of battery performance over time. As the performance decreases, the battery might not meet the requirements for usage as an EV battery and thus need to be switched out. The state of health (SoH) of an EV battery pack is often measured as $\frac{C_A}{C_N}$, where C_A and C_N represent the available capacity and the nominal capacity, respectively. If or when the SoH drops below a certain level, often $70 - 80\%$, the battery is replaced and evaluated for a second life use or recycling.

Second Life - The concept of a second life in EV batteries stems from retiring these batteries and repurposing them in different use cases. Batteries are tested and analyzed to determine whether they are eligible for a different use case or if they are in their end of life cycle and are to be recycled. The batteries can be repurposed for a multitude of tasks, two examples being charging stations and residential photovoltaic energy storage systems [2].

Batteries that have degraded past their use case in a second life are completely discharged and recycled. The capacities of the batteries are often unknown and to ensure that the temperature doesn't increase to problematic levels, the batteries are currently discharged at a relatively low rate while switching between CC and CV stages. Optimizing this process could save time but also imply complications regarding thermal stress on the battery. Intelligent modeling of the batteries and implementation of control algorithms could potentially reduce the time needed for a complete discharge while maintaining safe temperature levels.

One important aspect of battery recycling is pretreatment. The pretreatment process contains multiple steps, including discharge, dismantling, communition, classification, separation followed by dissolution, and thermal treatment [3]. This project focuses on effectivizing the discharging step. There are different methods of pre-

treatment of Li-ion batteries currently in use and in a paper by Shi et. al., four methods were investigated and compared in terms of aspects such as battery model adaptability, discharge efficiency, and waste emission level [4]. The compared methods of discharge were controlled passivation, saline discharge, discharging through use of conductive metal powder, and load circuit discharge. Load circuit discharge is highly compatible with control strategies, as electrical models are widely used in control applications. To optimize the discharge process, this thesis focuses on controlling load circuit discharge.

1.1 Purpose

The current industry standard process of discharging batteries which are going to be recycled is intended to prioritize safety and minimize the risk of excessive degradation which may lead to thermal runaway. Since the capacities and the respective SoH is often unknown, the maximum temperature which would be deemed as safe during discharge may vary between batteries and may differ from the limit stated by the manufacturer. To achieve a safe discharge, the process uses a relatively low discharge rate with the intent of keeping the internal temperatures in the batteries from rising to problematic levels. This method could be seen as somewhat rudimentary given that the temperatures during discharge could be higher without causing excessive damage to the batteries at the expense of causing a slow process with regard to discharge time. Furthermore the temperature measurements only act as safeguards to interrupt the discharge if the temperatures exceed their set limits.

With regards to the projected increase in demand for LIB in the future, a small increase in efficiency during the discharge portion of the recycling and pretreatment phases could imply a noticeable benefit in decreasing cost of labour and time.

The purpose of this work is to create a discharge cycle that utilizes the temperature measurements in a control loop such that the discharge time decreases, while a safe temperature level is maintained, to optimize the trade-off between a fast discharge policy while maintaining a safe work environment. A paper from Kawakita de Souza et. al. [5] utilizes MPC and a low-level equivalent circuit model (ECM) to manage cell performance for charging of lithium-ion batteries (LIBs), and based on this paper it would seem likely that MPC could also be used for the discharging process during recycling.

2
Objective and Scope

This section presents the goal of the project, along with limitations and the scope definition. The aim of this section is to provide an understanding of focal points of the project and to clarify points that are not researched but could be influential to the work.

2.1 Objective

The research questions which will be investigated during this thesis are

- How effective are the four different control strategies CC-CV, CC-CT, DP and robust MPC at minimizing discharge time while ensuring that temperature constraints are maintained for both cell-level and module-level battery systems?
- How does the use of a cell-level equivalent circuit model (ECM) with thermal modeling perform as a module-level prediction model in terms of discharge time optimization and temperature management?

The objective of this study is to compare control strategies and determine to what degree the controllers could be used for the purpose of discharging batteries for recycling. Since the current method of discharging batteries is dependent solely on a CC stage, it is of industrial and academic interest to investigate how this process can be optimized, both with regards to time and safety.

2.2 Limitations

A facility which receives battery modules for discharging and transportation to recycling plants may receive batteries with different specifications and from different manufacturers. This study assumes homogeneity between battery models with no assumed specific characteristics within the batteries. The efficiency of control methods may differ based on the batteries internal structure but these effects will not be thoroughly researched in this project. The focal point of this work is on the controller, therefore there will not be a large focus on safeguards in accordance with safety protocol standards, apart from monitoring the temperature.

Because of the lack of experimental data and knowledge about the plant, given that there is no specific battery model tested, the temperature limit is set to 40 °C.

Since many variables such as SoH, safe operating voltage range and maximum allowed current are unknown, the temperature constraint is set relatively low with the intention of emphasizing the safety of the operation.

The model used for both the cell-level and module-level state dynamics and state estimation is based on an ECM with a zero-dimension lumped mass heat equation, which is explained further in Sec. 4.1.1. This is to simplify the modeling work necessary to evaluate the controllers, since the main focus of the project is the controller performance, as opposed to battery modeling.

In this project, there are no physical experiments to validate the results. The data is gathered, and the controllers are evaluated, using Simulink models of a battery, discharged by a Controlled Current Source block. This is an acceptable limitation, as the aim is to gather data using measurements during simulations to emulate the process for a real-world application.

2.3 Boundaries

This project focuses on optimizing the discharge cycle of EV batteries for recycling purposes. This implies that the batteries are not meant for redistribution or further use. There is no evaluation in this project on how well the controllers adapt to different battery models, chemistries, cell configurations or geometries. However, utilizing grey box modeling, the aspiration is to mitigate some challenges that may arise because of battery variations in a future scenario.

The control strategies are evaluated based on time to complete discharge and ability to not exceed the temperature threshold. A potential by-product of the project is that the control policies could be utilized for charging batteries, but this will not be a focal point during the project, and could thus be a potential subject for further research.

3
Theory

This section is aimed towards explanation of concepts that will be used and discussed in this master's thesis. Some subjects are included for clarification purposes and are thus meant to clarify the specific use cases in the context of this project.

3.1 Lithium Ion Batteries

The main problem with electrical abuse conditions such as high temperatures concerns that it may cause an external short circuit (ESC) [6]. ESC gives cause to a rapid increase in temperature which is primarily caused by ohmic heat generation and when a LIB reaches $77 - 121°C$, venting and electrolyte leakage may occur, which is identified by a drop in voltage and increased heat generation. When thermal runaway is triggered, the internal structure of the battery has changed and the battery is no longer safe to handle or discharge and needs to be disconnected and handled according to predefined safety measures. High current passing through a damaged battery may cause explosion of the cells and it is thus favourable to employ pre-emptive safety measures to avoid thermal runaway when discharging the batteries.

3.2 Modeling

When modeling a physical system for automatic control, the approach differs in relation to the level of understanding of the system's dynamics. Some concepts that are important to know about to understand this project are *white*, *black*, and *grey box* modeling techniques.

If the underlying mechanics of the system are well understood, it can be appropriate to utilize a *white box* model, often also referred to as *first principle modeling*. In this approach, the system dynamics are described using mathematical equations derived from physical principles. This way, a white box model can be accurate in predicting the system's response to inputs on the assumption that the equations describing the system are relevant and at an adequate level of detail.

If explicit knowledge of a system is lacking, or the dynamics are unknown, one can view the system as a *black box*, which relies on data to create a model. Here, instead of relying on fundamental principles to gain understanding of the system,

the inputs and outputs are studied and the gathered data is combined with statistical or machine learning techniques to infer input-output relations and predict system behavior. Since it is possible to vary the complexity of the model based on the data gathered, this approach is flexible in comparison to white box modeling at the expense of theoretical grounding and possibly interpretability.

Because of the complex structure of battery modules and lack of knowledge regarding placement of internal temperature sensors, heat dissipation and cooling, this project mainly focuses on utilizing so called *grey box* modeling techniques. This implies basing the model on mathematical formulations of electro-thermal dynamics, such as an ECM, and using simulation data to estimate parameter values. This approach is taken with the intention of being applicable to batteries from different manufacturers and internal structures, while still aiming to provide accurate control of the temperature during a discharge cycle and minimizing the need for large sets of simulation data to fit the model.

3.2.1 Equivalent Circuit Model

The electrical modeling of a battery cell is realized through an ECM. The electrical model consists of a voltage source, acting as the open-circuit voltage (OCV), a resistor, R_0, representing the internal resistance and a parallel resistor-capacitor (RC) pair to model the time dynamics of the system, referred to as R_1 and C_1, respectively. A diagram of the electrical circuit can be seen in Fig. 3.1.

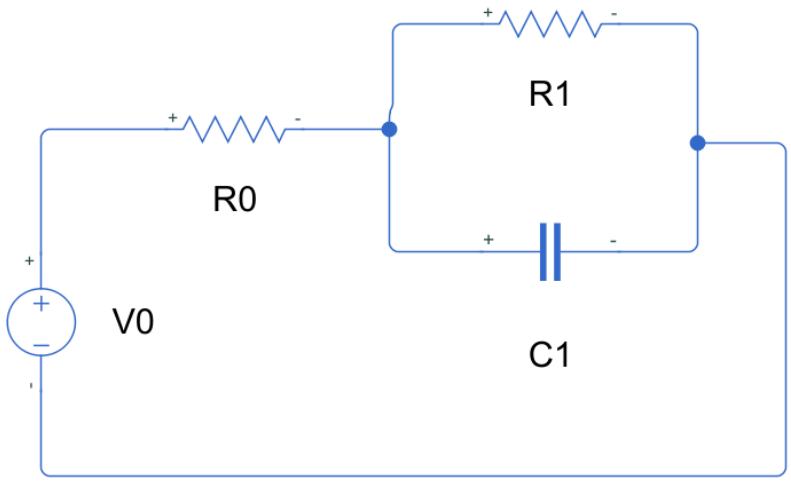

Figure 3.1: Electrical diagram of the ECM used for modeling the battery cell

When modeling a battery using an ECM, it's possible to use multiple parallel RC pairs in series to more accurately model the time dynamics. Multiple RC pairs could be especially beneficial to the model accuracy when the system will be subjected to rapid changes in input current. Conversely, with an input current that varies slowly or remains relatively stable over time, the system will be in a quasi-steady state, implying that the transient effects become negligible compare to the overall operating

conditions. In terms of model complexity, estimating parameters, and computing power, it is of interest to balance model accuracy and computational complexity. In this project, the input current's rate of change was relatively low during a discharge cycle which implies that one RC pair should be sufficient to model the system dynamics.

The states required to describe the ECM is state of charge (SoC), voltage over the RC pair, referred to as V_1, surface temperature, T_s, and core temperature, T_c. The mathematical model is described by the system of differential equations:

$$\frac{dSoC(t)}{dt} = -\frac{I(t)}{3600C_n} \tag{3.1}$$

$$\frac{dV_1(t)}{dt} = -\frac{V_1(t)}{R_1C_1} + \frac{I(t)}{C_1} \tag{3.2}$$

$$\frac{dT_s(t)}{dt} = \frac{T_f - T_s(t)}{R_uC_s} - \frac{T_s(t) - T_c(t)}{R_cC_s} \tag{3.3}$$

$$\frac{dT_c(t)}{dt} = \frac{T_s(t) - T_c(t)}{R_cC_c} + \frac{I(t)}{C_c}\Big[V_1(t) + R_0I(t)\Big] \tag{3.4}$$

where I is the input current, C_n the nominal capacity of the battery cell, R_u and R_c convection and conduction resistance, respectively, T_f the ambient temperature, and C_s and C_c the surface and core heat capacity, respectively [7].

3.2.2 State of Energy Estimation

One of the metrics on which the different discharge strategies are evaluated is the time necessary for a complete discharge. The proposed method of determining when the battery is fully discharged is measuring the extracted energy from the battery and comparing it to the nominal energy, E_{nom}. The energy output is calculated as

$$E_{\text{output}} = \int_0^t V_{\text{T}} I dt \tag{3.5}$$

where V_{T} is the terminal voltage and I is the load current drawn from the battery. The nominal energy is determined through the CC-CV discharge which acts as a benchmark for the other discharge methods. The state of energy (SoE) can be defined as

$$SoE(t) = 1 - \frac{E_{\text{output}}(t)}{E_{\text{nom}}} \tag{3.6}$$

which can be discretized as

$$SoE(k) = SoE(k-1) - \frac{\eta V_T(k-1)I(k-1)t_s}{E_{\text{nom}}} \tag{3.7}$$

where η denotes the energy efficiency of the battery, in this project set to $\eta = 1$, and t_s represents the sampling time of the system [8]. The SoE makes out the fifth

state of the battery dynamics and the state evolution is referred to using

$$\mathbf{x}(k+1) = f(\mathbf{x}(k), I(k)) = \begin{cases} A\mathbf{x}_i(k) + BI(k), & i \in (1,2,3,4) \\ x_5(k) - \frac{\eta V_T(k-1) I(k-1) t_s}{E_{\text{nom}}}, & \text{(SoE update)} \end{cases} \tag{3.8}$$

where A and B are state-space matrices. How these matrices are derived is discussed in Sec. 3.2.3.

3.2.3 State-Space Representation and Discretization

Linearization is a method of creating a linear approximation of the differential equations defining the system dynamics at an operating point, $(\mathbf{x}_{\text{op}}, \mathbf{u}_{\text{op}})$. By describing the differential equations modeling the state dynamics as

$$\dot{\mathbf{x}}(t) = \mathbf{f}(\mathbf{x}(t), \mathbf{u}(t)) \tag{3.9}$$

$$\mathbf{y}(t) = \mathbf{h}(\mathbf{x}(t), \mathbf{u}(t)) \tag{3.10}$$

and by assuming small deviations, a first-order Taylor expansion can be conducted which yields

$$\dot{\mathbf{x}}(t) + \dot{\Delta\mathbf{x}}(t) = \mathbf{f}(\mathbf{x}(t), \mathbf{u}(t)) + \left.\frac{\partial \mathbf{f}}{\partial \mathbf{x}}\right|_{\mathbf{x}_{\text{op}}, \mathbf{u}_{\text{op}}} \Delta\mathbf{x}(t) + \left.\frac{\partial \mathbf{f}}{\partial \mathbf{u}}\right|_{\mathbf{x}_{\text{op}}, \mathbf{u}_{\text{op}}} \Delta\mathbf{u}(t) + \mathcal{O}(||\Delta\mathbf{x}||^2, ||\mathbf{u}||^2) \tag{3.11}$$

$$\mathbf{y}(t) + \Delta\mathbf{y}(t) = \mathbf{h}(\mathbf{x}(t), \mathbf{u}(t)) + \left.\frac{\partial \mathbf{h}}{\partial \mathbf{x}}\right|_{\mathbf{x}_{\text{op}}, \mathbf{u}_{\text{op}}} \Delta\mathbf{x}(t) + \left.\frac{\partial \mathbf{h}}{\partial \mathbf{u}}\right|_{\mathbf{x}_{\text{op}}, \mathbf{u}_{\text{op}}} \Delta\mathbf{u}(t) + \mathcal{O}(||\Delta\mathbf{x}||^2, ||\mathbf{u}||^2), \tag{3.12}$$

and using Eq. 3.9 and Eq. 3.10, Eq. 3.11 and Eq. 3.12 can be equivalently written as

$$\dot{\Delta\mathbf{x}} \approx \mathrm{A}\Delta\mathbf{x}(t) + \mathrm{B}\mathbf{u}(t) \tag{3.13}$$

$$\Delta\mathbf{y}(t) \approx \mathrm{C}\Delta\mathbf{x}(t) + \mathrm{D}\mathbf{u}(t) \text{ [9].} \tag{3.14}$$

This state-space representation can be used as a linear approximation of the system dynamics, and its lower computational complexity as opposed to the nonlinear differential equations is suitable for implementation in state estimation and MPC.

Controllers, such as MPC, typically operate in discrete time, however, so for this to be useful in a control environment, it is necessary to discretize the system dynamics. This can be done by approximating the continuous differential equations with difference equations over discrete time steps of sampling time t_s. The continuous-time state-space model described by Eq. 3.13-3.14 can be discretized using zero-order hold, where control inputs are assumed constant during each sampling interval. This generates the discrete-time state-space model

$$\Delta\mathbf{x}(k+1) = \mathrm{A}_d\Delta\mathbf{x}(k) + \mathrm{B}_d\mathbf{u}(k) \tag{3.15}$$

$$\Delta\mathbf{y}(k) = \mathrm{C}_d\Delta\mathbf{x}(k) + \mathrm{D}_d\mathbf{u}(k) \tag{3.16}$$

where A_d, B_d, C_d, and D_d are the discrete-time state-space matrices, and k represents the discrete time step. The discrete-time state-space matrices can be computed using the continuous-time state-space matrices as

$$A_d = e^{At_s} \tag{3.17}$$

$$B_d = \int_0^{t_s} e^{A\tau} d\tau B \tag{3.18}$$

$$C_d = C \tag{3.19}$$

$$D_d = D \text{ [10].} \tag{3.20}$$

These expressions can be computed numerically, and functions such as `c2d` in MATLAB compute the discrete-time state-space given a continuous-time state-space. This discrete-time state-space model is now suitable for use in predictive controllers such as DP and MPC.

3.3 Control Strategies

The implementation of each controller is discussed in Sec. 4.2. This section aims to discuss the theory necessary to understand how each controller operates.

3.3.1 CC-CV

A proposed method to measure the nominal energy, E_{nom} in a battery is to discharge the battery from fully charged by a CC stage, until a lower cut-off voltage is reached, followed by a CV stage, until a lower cut-off current is reached [8]. A battery being fully charged is determined by information on the specific battery cell's, or module's, documented nominal voltage. Likewise, the lowest safe operating voltage is also determined by information from a data sheet. Because of the limitations of the project, and the absence of real-world measurement data from experiments, the Simulink table-based battery cell model and battery module created using MATLAB's Battery Builder application, which are used as plants, are assumed to be fully charged at the start of the simulation, and the lower cut-off voltage is chosen based on the available tabulated data from the Simulink models.

3.3.2 CC-CT

The use of a CC-CT discharge scheme is based on experimental results showing that discharging a battery at a higher temperature yields a lower residual energy after a complete discharge [11]. The initial CC stage is equal to that of the CC-CV discharge strategy, which lasts until the estimated cell core temperature, or the maximum internal temperature of the model, reaches a temperature threshold. The controller then switches to a PI control scheme to maintain a temperature setpoint until the battery is fully discharged.

3.3.3 DP

DP is a method of solving complex optimization problems by decomposing them into sub-problems. It relies on the principle of optimality, stating that the optimal solution to a problem can be constructed from optimal solutions of its sub-problems [12]. The DP approach to control, in the context of battery discharge optimization, is to determine the optimal discharge current profile that minimizes an objective function, while adhering to constraints on the states and inputs. The objective function is often based on penalties applied to the states and the input, and the problem can be formulated as

$$\min_{I} \quad \mathcal{J}_{\text{DP}} \tag{3.21}$$

subject to

$$\mathbf{x}(k+1) = f(\mathbf{x}(k), I(k)), \quad k = 1, 2, \ldots, t_f \tag{3.22}$$

$$\mathbf{x}(0) = \mathbf{x}_0 \tag{3.23}$$

$$\mathbf{x}_{\min} \leq \mathbf{x}_k \leq \mathbf{x}_{\max}, \quad k = 1, 2, \ldots, t_f \tag{3.24}$$

$$\mathbf{u}_{\min} \leq \mathbf{u}_k \leq \mathbf{u}_{\max}, \quad k = 1, 2, \ldots, t_f \tag{3.25}$$

where f is a function describing the state dynamics, $\mathbf{x}_0$ describes the initial condition, and $\mathbf{x}_{\min}$, $\mathbf{x}_{\max}$, $\mathbf{u}_{\min}$, $\mathbf{u}_{\max}$ describe the constraints. The problem can then be formulated according to specific guidelines for a solver, which iteratively calculates the cost function and generates the optimal discharge current based on the defined problem formulation.

3.3.4 MPC

MPC is a constrained-based control approach that considers a predefined number of time steps in the future, referred to as the horizon N, and calculates the optimal control policy based on minimizing the penalties on the future states and control actions, similar to DP. This is combined with constraints on the states and control signal based on predefined sets for each quantity such that the control policy does not violate these constraints. The optimal control policy for time step k is calculated by minimizing the objective function

$$\min_{\mathbf{u}_{0:N-1}} \mathcal{J}_N + \sum_{k=0}^{N-1} ||\mathbf{x}(k) - \tilde{\mathbf{x}}||^2_{\mathrm{Q}_\mathbf{x}} + ||\mathbf{u}(k) - \tilde{\mathbf{u}}||^2_{\mathrm{Q}_\mathbf{u}} \tag{3.26}$$

subject to

$$\mathbf{x}(k+1) = f(\mathbf{x}(k), \mathbf{u}(k)), \quad k = 1, 2, \ldots, N \tag{3.27}$$

$$\mathbf{x}(0) = \mathbf{x}_0 \tag{3.28}$$

$$\mathbf{x}_{\min} \leq \mathbf{x}(k) \leq \mathbf{x}_{\max}, \quad k = 1, 2, \ldots, N \tag{3.29}$$

$$\mathbf{u}_{\min} \leq \mathbf{u}(k) \leq \mathbf{u}_{\max}, \quad k = 1, 2, \ldots, N \tag{3.30}$$

and applying the input $\mathbf{u}(0)$ to the plant, where $\mathcal{J}_N$ denotes the terminal state cost, $\mathbf{x}(k)$ the state of the system at time step k, $\mathbf{u}(k)$ the control signal at time step k, $\mathbf{x}_0$ the initial condition, $\tilde{\mathbf{x}}$ the state setpoints, $\tilde{\mathbf{u}}$ the control setpoint, $\mathrm{Q}_\mathbf{x}$ and

$\mathrm{Q}_{\mathbf{u}}$ penalty matrices for the state and control signal, respectively, and f a function describing the system dynamics. This process is repeated at every time step, under the assumption that there exists a set of inputs that does not cause violation of any constraints. To mitigate the risk of MPC not being able to generate a feasible input, it is possible to soften the constraints or switch to a different control method.

Tube-based MPC extends the MPC framework to add robustness to disturbances. This is achieved by incorporating an additional controller, such as the linear-quadratic regulator (LQR). This can be implemented by setting a disturbance bound, d_{db}, and calculating the LQR optimal control gain, $\mathrm{K}_{\mathrm{LQR}}$, obtained by state and control weight matrices $\mathrm{Q}_{\mathrm{LQR}}$ and $\mathrm{R}_{\mathrm{LQR}}$. This results in the feedback control law, defined by the closed-loop dynamics

$$\mathrm{A}_{\mathrm{cl}} = \mathrm{A} - \mathrm{B}\mathrm{K}_{\mathrm{LQR}}, \tag{3.31}$$

where A and B are state-space matrices. The impact of disturbances on the system states can then be calculated to account for the maximum expected disturbance. The disturbance impact for each state, d_i, is calculated as the sum of the absolute values of the elements in the i-th column of the closed-loop matrix A_{cl}, scaled by the disturbance bound:

$$d_i = \sum_{j=1}^{n_x} |(\mathrm{A}_{\mathrm{cl}})_{j,i}| \times d_{\mathrm{db}} \tag{3.32}$$

where n_x signifies the number of states, capturing the worst-case deviation for each state due to disturbances.

4
Method

Building on the theory of how the modeling was intended to operate (see Sec. 3), the aim of this section is for the reader to be able to recreate the experiments done in the project and further build upon the conclusions.

4.1 Data Collection and Modeling

Multiple controllers implemented in this project rely on state prediction and state estimation. This section explains how the modeling was conducted for this specific project and use-case.

4.1.1 State-Space Modeling

To generate cell-level data, a table-based battery cell model from the Simscape battery library was used, along with parameters from [7]. The additional parameters not included in [7] were estimated using discharge data from the plant. The model used electrical circuit elements and a zero-dimensional lumped-mass thermal heat equation to model the electro-thermal dynamics of a battery cell. Variable characteristics of the electrical circuit elements are tabulated as functions of SoC and temperature. Data on SoC and surface temperature was gathered using sequential discharge pulses of 30 A where the duration of the pulse was determined by each pulse discharging the battery equivalent to 10 % of the nominal capacity. Through the thermal model of the Simscape battery, the cell temperature was recorded during the discharge cycle and saved for estimation of model parameters (see Tab. 4.1).

By implementing the differential equations governing the electro-thermal dynamics of the battery model (see Sec.3.2.1-3.2.2) as a Simulink model, the Parameter Estimation toolbox was used to identify parameter values generating a model with optimal accuracy with regards to the governing equations used[1] (see Tab. 4.1). Lastly, the Model Linearizer toolbox was used to create a state-space model at the initial condition $\mathbf{x}_0 = \begin{bmatrix} 1 & 0 & 20 & 20 \end{bmatrix}^\top$ at a sampling rate of 1 Hz which generated

[1] Herein lies a distinction of using a gray box model. Since, although the parameter values are physically possible, the model could potentially be overfitted to the data, effectively generating a model with poor generality

the state-space matrices

$$\mathrm{A} = \begin{bmatrix} 1 & 0 & 0 & 0 \\ 0 & 9.9769 \times 10^{-120} & 0 & 0 \\ 0 & 0.0009 & 0.7727 & 0.1901 \\ 0 & 0.0044 & 0.0310 & 0.9683 \end{bmatrix}, \mathrm{B} = \begin{bmatrix} -3.5613 \times 10^{-6} \\ 0.0003 \\ 0.0008 \\ 0.0075 \end{bmatrix} \tag{4.1}$$

used for state estimation and the MPC controller. Note that the SoE is not included in the linearized state-space. Because of its importance of accuracy to the project and reliance on the terminal voltage, which is not included in the state-space, the SoE is calculated separately from the variables SoC, V_1, T_s, and T_c.

To gather module-level data, MATLAB's Battery Builder app was used to create a Simscape model of a battery module based on the LG Chem E78 pouch cell in a 12s2p configuration [13]. This cell was chosen on the basis that it is commonly used in EVs, such as the Volkswagen ID line [14]. The LG Chem E78 data was used to create a cell model and 12 cells were put in a series connection as a module, according to the Battery Builder terminology, and a battery pack was created by connecting 2 of these modules in parallel. The reason for creating a pack in this manner instead of a module based on cells and a parallel assembly of cells, was that outports such as SoC and internal cell temperature are only available for battery packs. The SoC and temperature data was gathered using a sequence of corresponding time-data values which were chosen based on an iterative process, selecting a discharge current, creating a state-space as done in the cell-level modeling, and choosing a new discharge current profile, based on the current generated from the MPC. The final current profile used for the data collection was

$$\mathbf{t} = \begin{bmatrix} 0 & 5000 & 10000 & 15000 & 20000 & 25000 & 30000 & 35000 \end{bmatrix} \tag{4.2}$$

$$\mathbf{I} = \begin{bmatrix} 26.0 & 25.2 & 24.4 & 22.75 & 22.2 & 21.6 & 21.25 & 20.9 \end{bmatrix} \tag{4.3}$$

showing the corresponding time-current values, given in seconds and amperes, which generated the state-space

$$\mathrm{A} = \begin{bmatrix} 1 & 0 & 0 & 0 \\ 0 & 0.1200 & 0 & 0 \\ 0 & 0.0002 & 0.9651 & 0.0132 \\ 0 & 0.0217 & 0.0002 & 0.9998 \end{bmatrix}, \mathrm{B} = \begin{bmatrix} -8.9031 \times 10^{-6} \\ 0.0018 \\ 9.5637 \times 10^{-7} \\ 0.0002 \end{bmatrix} \tag{4.4}$$

with a sampling time of 0.2 Hz. The ECM parameters were identified using the same method described for the cell-level data collection (see Tab. 4.1).

Table 4.1: Resulting parameter values after estimation from discharge data

Parameter	Value (Cell Model)	Value (Module Model)
C_1 [F]	12.6138	174.3546
C_c [J/K]	62.7000	2059.8844
C_s [J/K]	4.5000	31.8814
R_0 [Ω]	0.0099	0.0001
R_1 [Ω]	0.0003	0.0036
R_c [K/W]	1.9400	14.4802
R_u [K/W]	15.0000	8.8647

4.1.2 State Estimation and SoE

A Kalman Filter block was implemented as a state estimator for the Simulink simulations. The state estimator builds on the discrete state-spaces from Sec. 4.1.1. The Kalman filter is used for optimal state estimation by combining the model's prediction with real-time measurements, accounting for uncertainties in both. In each iteration, the filter operates in two main steps: the prediction step and the update step. During the prediction step, using the system's state-space model, the Kalman filter predicts the state $\hat{\mathbf{x}}(k|k-1)$ at time step k, given all measurements up to the previous time step $k-1$. The state prediction can be expressed as

$$\hat{\mathbf{x}}(k|k-1) = \mathrm{A}\hat{\mathbf{x}}(k-1|k-1) + \mathrm{B}\mathbf{u}(k-1). \tag{4.5}$$

Simultaneously, the error covariance $\mathrm{P}(k|k-1)$ of the prediction is updated as

$$\mathrm{P}(k|k-1) = \mathrm{A}\mathrm{P}(k-1|k-1)\mathrm{A}^T + \mathrm{Q}, \tag{4.6}$$

where Q represents the process noise covariance matrix. During the update step, once a new measurement $\mathbf{z}(k)$ is received, the filter adjusts the predicted state using the measurement residual, which is the difference between the actual measurement and its predicted value, expressed as

$$\mathbf{y}(k) = \mathbf{z}(k) - \mathrm{C}\hat{\mathbf{x}}(k|k-1), \tag{4.7}$$

where C is the observation matrix. The Kalman gain $\mathrm{K}(k)$ is then calculated to minimize estimation error by weighting this residual

$$\mathrm{K}(k) = \mathrm{P}(k|k-1)\mathrm{C}^T \left(\mathrm{C}\mathrm{P}(k|k-1)\mathrm{C}^T + \mathrm{R}\right)^{-1}, \tag{4.8}$$

where R is the measurement noise covariance. This gain determines the influence of the measurement on the state update, balancing model prediction against measurement reliability. The estimated state is then updated as

$$\hat{\mathbf{x}}(k|k) = \hat{\mathbf{x}}(k|k-1) + \mathrm{K}(k)\mathbf{y}(k), \tag{4.9}$$

and the error covariance $\mathrm{P}(k|k)$ is revised to reflect the updated estimate's uncertainty as

$$\mathrm{P}(k|k) = (\mathrm{I} - \mathrm{K}(k)\mathrm{C})\,\mathrm{P}(k|k-1) \tag{4.10}$$

where I is the identity matrix. This process iteratively refines the state estimate, using the model's dynamics in the prediction and real-time measurements in the update. The SoC output from the battery model and temperature measurement was used as measurements for the SoC and surface temperature, respectively, with noise covariances 0.3 for the states and 1 for the measurements. The SoE was calculated outside of the state estimator, using measurements on the load current, terminal voltage, and an Integrator block.

To estimate the SoE, information on the terminal voltage is needed. Since the internal resistance of the battery is assumed to be known from the parameter estimation, the OCV is needed to calculate the terminal voltage of the ECM. Based on the ECM, by discharging the battery models at a low current rate, following Ohm's law, it was assumed that $V_{\mathrm{T}} \approx V_{\mathrm{OCV}}$. The models were discharged at 0.02 C and the terminal voltage was compared to the SoC to create a nonlinear relation between SoC to OCV. A polynomial of degree 4 was fitted to the data using the MATLAB Curve Fitter toolbox which generates the polynomials

$$OCV(SoC) = p_1 SoC^4 + p_2 SoC^3 + p_3 SoC^2 + p_4 SoC + p_5 \tag{4.11}$$

where the parameters generated for the cell and module models can be seen in Tab. 4.2

Table 4.2: Polynomial coefficient values for OCV estimation as a function of SoC

Parameter	$\mathbf{p_1}$	$\mathbf{p_2}$	$\mathbf{p_3}$	$\mathbf{p_4}$	$\mathbf{p_5}$
Cell model	-2.0713	4.5787	-2.7974	0.9751	3.4939
Module model	-24.9533	55.1604	-33.8647	11.9152	41.5814

The battery dynamics could then be implemented as a MATLAB function in accordance to Eq. 3.8.

4.1.3 Model Validation

To evaluate the accuracy of the developed linearized model, a bounded random walk input current, limited between 0 A and 40 A, was applied to both the plants and the state-space models to capture dynamic system response. This randomized input enabled a direct assessment of the model's predictive accuracy. To quantify the accuracy, the relative Root Mean Square Error (RRMSE) was calculated for each measurable state, and the resulting accuracies can be found in Tab. 4.3. The RRMSE between two signals, y_1 and y_2, is calculated as

$$\mathrm{RRMSE} = \frac{\sqrt{\frac{1}{N}\sum_{k=1}^{N}(y_1(k) - y_2(k))^2}}{\sqrt{\frac{1}{N}\sum_{k=1}^{N} y_2(k)^2}}$$

where $y_1(k)$ represents the measured signal at time k, $y_2(k)$ represents the estimated signal at time k, and N represents the total number of samples. Using this metric to quantify the Root Mean Square Error of a signal relative to another provides

a normalized measure of fit. The states chosen to be compared are based on the ability to be measured, which for the cell-level plant were SoC, V_T, T_s, and SoE, and respectively SoC, V_T, T_s, T_c, and SoE for the module-level plant. It should be noted that, because RRMSE was used, the values in Tab. 4.3 are dimensionless.

Table 4.3: RRMSE values quantifying the error between state-space model predictions and plant output measurements

State	RRMSE (Cell Model)	RRMSE (Module Model)
SoC	8.504×10^{-5}	0.3705
V_T	0.0028	0.0228
T_s	0.3564	1.3826
T_c	N/A	0.2174
SoE	0.0020	0.4138

4.2 Controllers

Based on the theory behind each controller (see Sec. 3.3), this section is aimed at explaining how the control strategies were implemented for this specific project.

4.2.1 CC-CV

The current was controlled using a Controlled Current Source block in Simulink which was initially set to a constant 39 A. The terminal voltage of the plant was measured using a Voltage Sensor block and compared to a constant, set to 3.47 V, which caused a Switch block to change the CC stage to the CV stage, when the terminal voltage dropped below the threshold. This was realized through a proportional controller, determining the current based on the deviation of the terminal voltage from the setpoint of 3.45 V. The proportional controller was tuned to a gain of 2000, and the discharge stopped when the current dropped to 0.05 C, or 3.9 A.
For the cell-level simulations, the discharge current for the CC stage is set to 39 A, as the capacity of the table-based cell model is 78 Ah. For the module-level, a current of 0.5 C is not possible, because of the limitation on current of 40 A, and the current for the CC stage is instead set to 0.25 C, equal to the discharge current of the cell-level simulations.

4.2.2 CC-CT

The CC stage of the CC-CT controller was implemented in the same way as that of the CC-CV controller. The internal temperature is estimated using a Kalman Filter block, with state space matrices generated according to Sec. 4.1.1. When an estimated internal temperature close to 40 °C is reached, the Controlled Current Source switches from CC to a PI controller using the PID Controller block. The parameters for the controller was set to $P = 60$ and $I = 0.02$ for the cell control and $P = 200.0000$ and $I = 0.0061$ for the module control.

4.2.3 DP

The objective for using DP in this application was to calculate the optimal discharge current with regards to minimizing the SoE as quickly as possible without violating the temperature constraint, providing an offline solution to the optimal discharge problem. The problem formulation was intended to be as similar as possible to that of the MPC controller but due to how the code was implemented, the cost function was altered between the cell-level and module-level scripts. The script was intended to treat the current at each time step as individual variables, minimizing the time to 0 % SoE. Since the time to complete discharge is in the range of 10 000 s, the number of variables would cause a need for more processing power than what was available during the project, which led to instead using fewer variables, acting as current changes with a specified hold time. For the cell-level DP, the number of variables were set to 500, and the hold time to 20 s. For the module-level DP, the number of variables were set to 250 and the hold time to 140 s. The problem formulation used for the DP problem can be expressed as

$$\min_{I} \quad \mathcal{J}_{\text{DP}} = \begin{cases} N \times t_{\text{h}} + 10^5 \times |x_5(N \times t_{\text{h}})| + \frac{\int_0^{N \times t_{\text{h}}} I(t)\,dt}{10^5}, & \text{if } x_5(t) > 0 \; \forall t \\ 10 \times t_{\text{f}} + \frac{\int_0^{N \times t_{\text{h}}} I(t)\,dt}{10^5}, & \text{if } \exists\, t_{\text{f}} : x_5(t_{\text{f}}) \leq 0 \end{cases} \tag{4.12}$$

$$\text{s.t.} \quad \mathbf{x}(k+1) = f(\mathbf{x}(k), I(k)), \quad k = 1, 2, \ldots, N \times t_{\text{h}} \tag{4.13}$$

$$\mathbf{x}(0) = [1, 0, 20, 20, 1]^\top \tag{4.14}$$

$$x_4(k) \leq 40, \quad k = 1, 2, \ldots, N \times t_{\text{h}} \tag{4.15}$$

$$\mathbf{I} = [\underbrace{I_1, I_1, \ldots, I_1}_{t_{\text{h}} \text{ times}}, \underbrace{I_2, I_2, \ldots, I_2}_{t_{\text{h}} \text{ times}}, \ldots, \underbrace{I_N, I_N, \ldots, I_N}_{t_{\text{h}} \text{ times}}] \tag{4.16}$$

$$0 \leq I(k) \leq 40 \quad k = 1, 2, \ldots, N \times t_{\text{h}} \tag{4.17}$$

where N is the number of variables, t_{h} is the hold time, and $f(\mathbf{x}(k), I(k))$ is a function describing the state dynamics (see Eq. 3.8).

4.2.4 MPC

Since the goal of the controller is to discharge the battery as quickly as possible, the terms in the cost function were implemented to reflect both rapid discharge and control cost. The MPC was implemented using YALMIP, a MATLAB toolbox for optimization modeling [15]. The solver used for the quadratic programming problem in the MPC controller is MOSEK [16]. Taking into account the results from [11], showing that maintaining a higher battery temperature during discharge is beneficial for extracting energy out of the battery, an estimated core temperature setpoint of 40 °C was used. The cost function also penalizes the SoE of each time step with an additional terminal cost of the SoE at the end of the control horizon.

The tube-based MPC was implemented using a disturbance bound of $d_{\text{db}} = .4$ and the LQR optimal control gain was obtained by the state and control weight

matrices

$$Q_{\text{LQR}} = \begin{bmatrix} 10000 & 0 & 0 & 0 \\ 0 & 0 & 0 & 0 \\ 0 & 0 & 100 & 0 \\ 0 & 0 & 0 & 0 \end{bmatrix}, R_{\text{LQR}} = 1. \tag{4.18}$$

The core temperature disturbance impact for the cell- and module level controllers were calculated to be $d_4 = 0.4843$, and $d_4 = 0.4062$, respectively. The MPC problem formulation could then be expressed as

$$\arg \min_{I(k:k+N)} \quad \mathcal{J}_{\text{MPC}} = 1000 \times x_5(N) + \sum_{k=1}^{N} \Big(10 \times (x_4(k) - 40)^2 + 100 \times x_5(k) \Big) \tag{4.19}$$

$$\text{s.t.} \quad \mathbf{x}(k+1) = f(\mathbf{x}(k), I(k)), \quad k = 1, 2, \ldots, N \tag{4.20}$$

$$0 \leq x_5(k) \leq 1, \quad k = 1, 2, \ldots, N \tag{4.21}$$

$$x_4(k) \leq 40 - d_4, \quad k = 1, 2, \ldots, N \tag{4.22}$$

$$0 \leq I(k) \leq 40, \quad k = 1, 2, \ldots, N \tag{4.23}$$

which was implemented as an interpreted MATLAB function.

5

Results

Following the simulations, this section presents relevant data and plots for key variables during the discharge process of the battery models. The results are separated into cell and module results.

5.1 Cell Results

The current profile generated using DP achieved the shortest discharge time out of the tested discharge methods, completing the discharge in approximately 2 h and 29 min. The discharge times for the remaining methods, listed in increasing order, are as follows: CC-CT, MPC, and CC-CV. A detailed comparison of discharge times for each method is provided in Table 5.1.

Table 5.1: Discharge times for the tested discharge methods in cell-level simulations, ordered by ascending time to complete discharge

Discharge Method	**Discharge Time**
DP	2 h 29 min
CC-CT	3 h 0 min
MPC	3 h 2 min
CC-CV	4 h 10 min

The simulations using the different discharge strategies for the cell level model show that a CC stage of 0.5 C could increase the estimated internal temperature of the battery to a level notably exceeding the temperature limit of 40 °C (see Fig. 5.1). The CC-CT simulation shows similar cell-level current control to MPC with the most notable difference being that the CC-CT discharge method violates the temperature constraint of 40 °C. This comparison can be seen more clearly in Fig. 5.2.

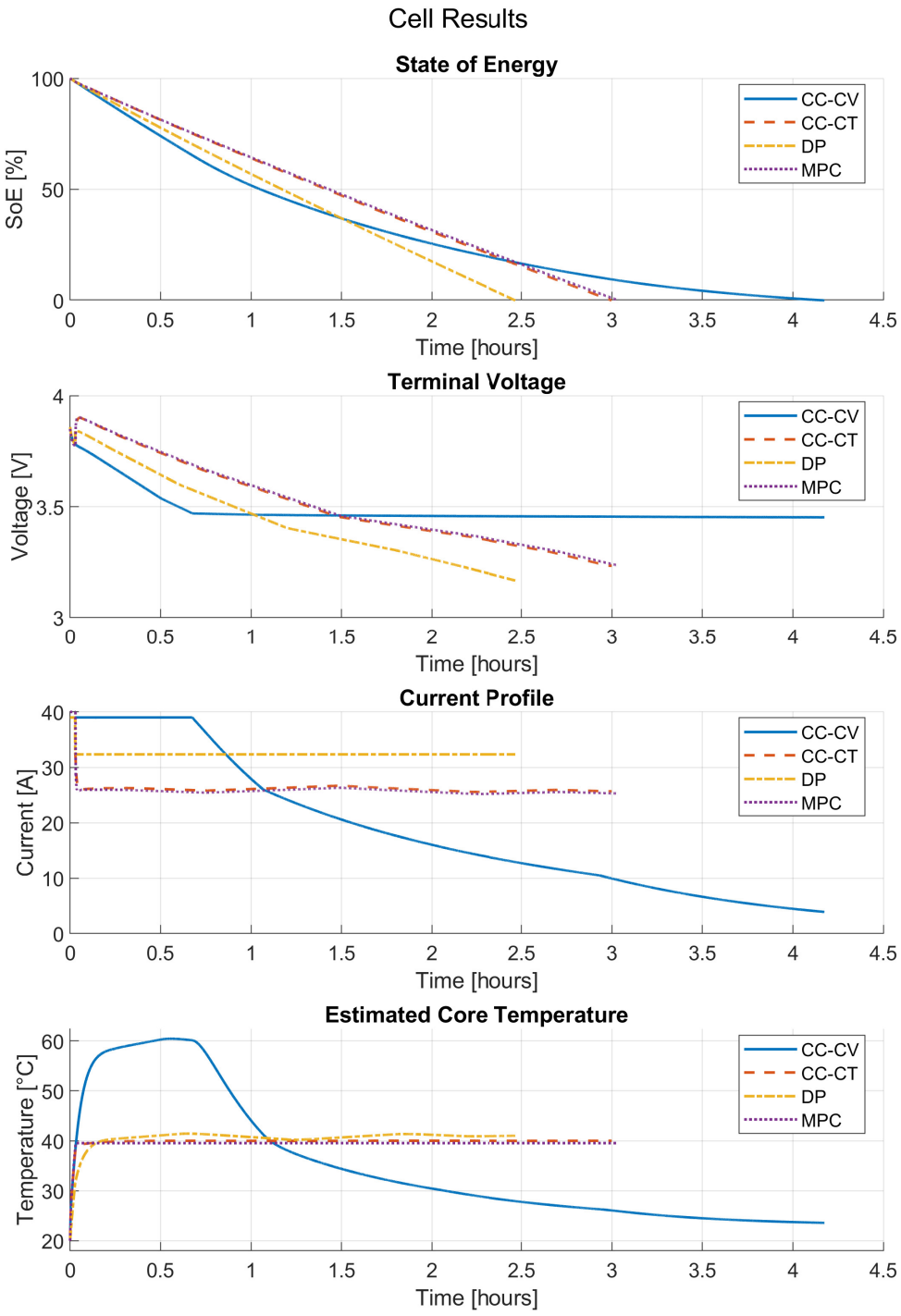

Figure 5.1: Battery cell simulation data for different discharge methods

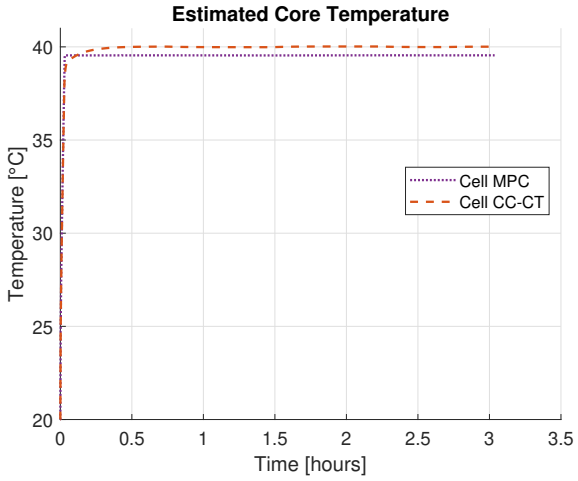

Figure 5.2: Estimated core temperature comparison between MPC and CC-CT controllers during cell-level simulations.

5.2 Module Results

For the module-level results, the CC-CV controller achieved the shortest discharge time, completing the discharge in 6 h and 4 min. The discharge times for the remaining controllers, listed in increasing order, are as follows: CC-CT, MPC, and DP. A detailed comparison of discharge times for each method is provided in Tab. 5.2.

Table 5.2: Discharge times for the tested discharge methods in module-level simulations, ordered by ascending time to complete discharge

Discharge Method	Discharge Time
CC-CV	6 h 4 min
CC-CT	6 h 33 min
MPC	6 h 38 min
DP	9 h 48 min

The simulation results show that the CC-CV and CC-CT controllers both violate the temperature constraint for prolonged periods of time, while the DP and MPC controllers manage to maintain a core temperature below 40 °C (see Fig. 5.3). The current generated from the DP controller was highly sensitive to modifications to the cost function and the initial guess. Moreover, the extended discharge time, compared to the other controllers, may indicate that the problem formulation or prediction model causes difficulties for the solver in finding the optimal solution.

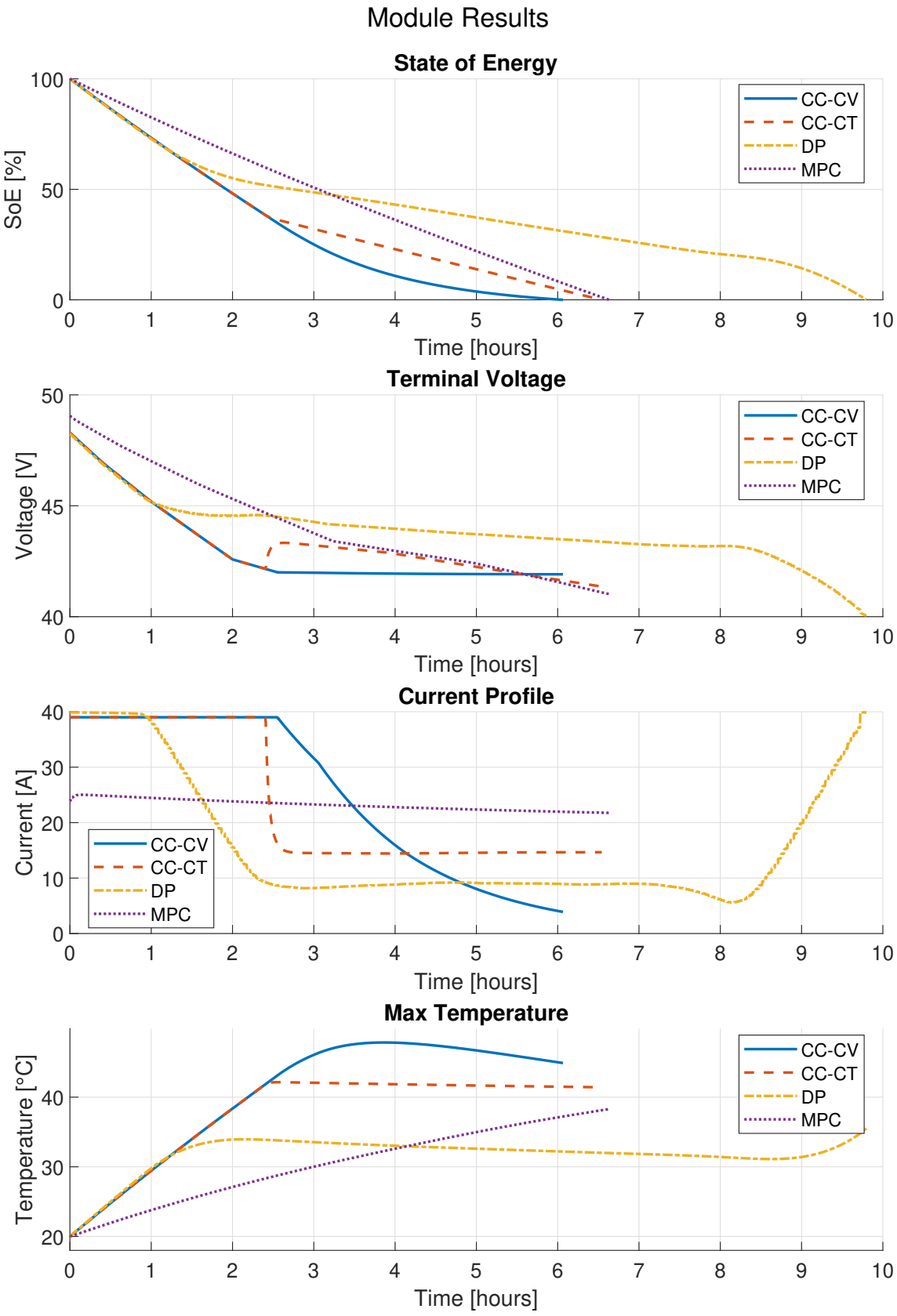

Figure 5.3: Battery module simulation data for different discharge methods

6
Discussion

The results from the cell-level simulations and the module-level simulations indicate that the controllers have varying degrees of adaptability when scaling from cell to module, and that there is a trade-off between simple controllers performing similarly during the different levels but could cause issues with safety without additional safeguards in place. Following the results from the simulation, this section aims to provide insights from the implementation and simulations on how well the controllers are suited for the application of battery discharge for recycling.

6.1 Modeling and Parameter Estimation

The data generated for the cell-level modeling is produced by a table-based battery model. The electro-thermal dynamics are therefore simplified as opposed to gathering data from a real battery cell. One implication of this is that there may be nonlinearities in a real battery cell that would not be accounted for in full by the Simulink model. More specifically, a table-based model is typically better suited for modeling systems resembling battery usage in a real-world application instead of deep discharging, pushing the limits of the cell in terms of temperature, energy extraction and voltage. With these limitations there are bound to be irregularities between results from simulations and results from experiments using a real battery.

Using a mathematical model expressing the electro-thermal dynamics of a battery cell to control a plant consisting of a battery module is inherently problematic. The results indicate a significantly less accurate performance for the module-level control when compared to the cell-level results. It is possible to note from Tab. 4.3 that the state-space model representing the cell-level plant can, with adequate accuracy, predict system behavior. This made a compelling argument to utilize the same methodology for the module-level plant. The RRMSE values for the module-level plant do show, however, that there is a significant mismatch between model and plant, especially regarding the surface temperature. This could be a consequence of a nonlinearity not being represented by the linearized state-space model. The higher accuracy for the core temperature estimates complicates the argument of whether or not the ECM is an appropriate model for this application. Based on the MPC results, it is possible to say that the module-level state-space model is conservative in core temperature. This implies a greater safety barrier, which is useful for the argument of workplace, and environmental, safety, but could also imply that there is a potential for faster discharge not being fully utilized.

6.2 Controller Performance

The controller performance is an important evaluation for this project and this section is aimed at discussing the results as well as how the controllers compare to each other.

6.2.1 CC-CV

The main metrics of interest in this project are the time to complete discharge and ability to maintain a safe temperature, not exceeding the temperature threshold. The CC-CV discharge strategy was meant to represent what is currently used in the industry where a battery module is often discharged using a single CC stage, followed by a short-circuit of the terminals. This method of discharge is highly sensitive to the battery capacity, and the heat generation could differ between batteries based on cell geometry and battery chemistry. The results from the simulation show that for both the cell and the module, the 40 °C threshold is exceeded. For some batteries, it could be safe to exceed temperature limits for a short period of time, but based on the premise of safely discharging batteries with regards to the ability to reuse the battery or the recycled battery materials, and employees handling the batteries, the CC-CV method of discharge could potentially cause thermal issues, such as a thermal runaway, possibly posing a risk for the facility and its employees.

6.2.2 CC-CT

The cell-level simulation results from the CC-CT discharge show that the controller causes the estimated core temperature to oscillate around the temperature threshold (see Fig. 5.1). The controller is relatively simple to implement. If core temperature measurement is feasible, or if the surface temperature is used for setpoint tracking instead, it could be a valid controller to consider for this application. However, basing the temperature setpoint on the estimated core temperature could be problematic for the same reasons as for the MPC, DP, or any other controller utilizing state estimation and is dependent on an accurate mathematical model. The module-level results indicate that the thermal mass is too high in relation to the heat dissipation for the module to stay below 40 °C when switching between the two stages (see Fig. 5.3). This is one issue with the CC-CT controller, that for it to stay below the threshold, it is necessary to switch to temperature setpoint tracking at a temperature lower than the threshold in order to not violate the constraint. This is relevant to another possible problem with the CC-CT controller. By the nature of the PI control, the proportional and integral gain parameters of the controller dictate the generated current. The integral coefficient could also cause wind-up effects if not tuned correctly, which may cause issues as those seen in the results. Furthermore, if the proportional coefficient is tuned too low, the temperature may not exceed the setpoint, but instead takes a longer time to discharge the battery. If the controller is tuned with a high proportional coefficient, overshooting may occur as can be seen in Fig. 5.3. This implies that a possible outcome of using a CC-CT controller is that the response is too slow, causing a loss in time, or that the response is too

aggressive, causing the temperature to exceed its intended setpoint. In this sense, it is difficult to tune the controller to an optimal level, minimizing the time spent discharging, while also maintaining robustness against constraint violations. There is also the possible case of introducing a steady-state error, where there is a notable drift caused by the CC-CT controller. This is also a factor to take into account when considering the effectiveness of PI control as opposed to MPC. Considering the discharge time data in Tab. 5.2 and the temperature plots in Fig. 5.3, it should be noted that the CC-CT controller discharges the battery quicker than the MPC with a difference of 5 min, but maintains a temperature over the limit for approximately 4 h, whereas the MPC never violates the temperature constraint.

6.2.3 DP

Using the DP solution as the discharge current proved problematic for multiple reasons. By calculating the discharge current off-line before discharge, the resulting discharge time and feasibility are entirely dependent on the accuracy of the prediction model. The cell-level results show similarities between DP and MPC, where the DP simulation discharges the battery faster, but at the cost of violating the temperature constraint due to model mismatch. The issue with the predictive model is apparent in the module-level results as well. The solution would come out as infeasible after the optimization, and the simulation would not encounter the same issue. This can be seen in the temperature plot, where the temperature is low in comparison to the other methods. There could be an issue with the problem formulation as well. The solution is sensitive to how the variables and hold times are constructed and defined. Decreasing the time window of the problem, effectively trying to reach 0 % SoE faster, would result in a more aggressive current profile, but since the prediction model is conservative in temperature, the generated current profile would tend to result in a longer discharge time than expected. For DP to be a controller to consider for an industry application, there would need to be further work done to ensure model accuracy, and a revision of the problem formulation and cost function is encouraged.

6.2.4 MPC

At both cell- and module-level, the MPC manages to maintain a temperature lower than the constraint. There is, however, a significant difference in generated current profile in the cell-level simulation, compared to the module-level. For the cell simulation, the current profile is similar to that of the CC-CT controller, prioritizing a high current, whereas for the module, the current is lower overall during the simulation. Since the cost function is identical in both simulations, one possible explanation for the difference in current profiles is connected to the calculation of the SoE. The battery module being in a 12s2p configuration, has twice the capacity, and a terminal voltage 12 times that of a single cell. Consider Kirchhoff's voltage law applied to the ECM. The terminal voltage would be expressed as

$$V_T = V_{\text{oc}} - R_0 * I - V_1, \tag{6.1}$$

implying that discharging a battery with a higher current reduces the terminal voltage as opposed to using a lower discharge current. This is visible in Fig. 5.3 in the terminal voltage plot. Given that there is penalty on the control input as well as the SoE and temperature, the lower current could be a result of the quadratic programming solution to the cost function. Another explanation could be that the prediction model is conservative in temperature and by extension causes the controller to generate a lower current as to not violate the temperature constraint. Since the temperature never reaches the constraint, and the MPC solution differs from the CC-CT it is difficult to draw a clear conclusion as to which of the explanations is the most plausible. Further research using a more accurate module model is recommended in order to make further arguments and to draw a more informed conclusion.

6.3 Sustainability

The Directorate-General for Environment of the European Union states that by the year 2030, EVs are expected to reach a total market share of 16% [17]. In the same article, it is estimated that supporting the power grid with second life batteries could avoid up to 1.2 kilotons of battery waste. Optimizing the cycling of these batteries is a natural step towards evolving the process of evaluating batteries for a second life or recycling.

The risk of thermal runaway poses not only a risk to the workers involved but also a negative environmental aspect. A battery module that has undergone thermal runaway may not be eligible for recycling to the same extend as a battery which hasn't. Furthermore, using control systems to adjust the discharge rate may also require a higher energy consumption when running, and in the case of using a real battery as opposed to a simulation, this implies additional required energy resources as opposed to the current industry standard.

To avoid thermal runaway during the charging cycle, the results from this study suggest that the allocated time for battery cycling could be reduced by using robust and predictive control schemes, such as MPC, compared to the industry standard, provided the same temperature constraints are imposed. By preventing thermal runaway and minimizing the degradation of the battery, the aspiration is that the environmental impact of this work will be a net positive in the process of battery recycling.

6.4 Ethics

It is important that the people working with examining the batteries are adequately safeguarded from possible danger regarding cycling used batteries. There are already safety precautions taken to ensure that people do not get hurt and by avoiding thermal runaway, this project aspires to further decrease the risk of excessive degradation that may lead to thermal runaway.

In a potential second life of the batteries, there must also exist a safety protocol to determine that the batteries are safe to use after cycling. This is especially crucial should the batteries be used for energy storage to support the power grid or in residential areas. This project does not, however, aim to produce these safety guidelines and this is therefore out of the scope of this thesis.

It is possible that necessary data from EV batteries is not publicly available if the information is considered sensitive. In this scenario, a possible mitigation strategy is to create a model for the thermal profile of the battery ourselves. This implies that there may be need for additional safeguards to ensure robustness and reliability and it may require further analysis into what precautions are necessary to provide a safe baseline for the discharge.

6.5 Future Work and Research

In the industry, the method of discharge is often not controlled more rigorously than by using a single CC stage, followed by short-circuiting the battery. This section is aimed at discussing what areas could be expanded upon, what steps to take in order to optimise the amount of time needed for discharge, and how to improve the safety of the discharge facility and the workers involved in the process.

6.5.1 Modeling

There is potential for improvement in the thermal modeling. For the cell-level, it could be of interest to investigate how a more detailed model would benefit discharge control. One example of such a model for cylindrical cells was developed by Richardson et al., describing the temperature distribution of a cylindrical cell using the Chebyshev spectral-Galerkin method [18]. The module-level results indicate that the model used for state estimation and prediction is inaccurate and in need of revising.

If these discharge methods were to be used in an actual facility, it would be interesting to investigate the range of accuracy the model has with regards to battery cell geometries and module configuration. If experiments are made on a battery module to enhance the model, there is precedent to investigate the level of accuracy the model would have if the discharge data is taken from a 12s2p pouch module, and then used on a 8s3p configuration of the same cell geometry, for example.

The data gathered for the modeling was based on models using tabulated data to represent the plant. The way the data was generated for the project could influence the control policies if the model poorly describes the system. When utilizing a linearized model around a specific operating point, the gathered data from the plant, the method by which the data was generated, and the chosen operating point influence the model's region of accuracy. Gathering data from different methods of discharge could help create a more accurate model.

6.5.2 Control Strategies

This project has implemented and tested different controllers with varying degrees of complexity, and there is potential for further development of the control. If safety is a priority for a project building on this thesis, it would be advisable to conduct an in-depth robustness analysis to ensure that the temperature does not exceed a specified threshold. The tube-based MPC could be a starting point, but disturbance impacts should be determined based on experimental data, and improved model accuracy could also increase the safety of the discharge process.

Aside from MPC, there could be interest in implementing stochastic optimisation algorithms, such as a genetic algorithm (GA). This was briefly tested during the project but was not included in the thesis due to time constraints. If the current profile is viewed as a sequence of current changes with zero-order hold, the problem is well-suited for GA implementation, representing current profiles as chromosomes and sequences of current changes as genes. This implementation is similar to that of DP, as the problem formulation and cost function heavily influence the resulting current profile. Further investigation into the cost function, both for MPC and DP, is also strongly encouraged based on the project results. It should be noted that, while it could be valuable to explore AI-based control and assess the potential of approaches such as reinforcement learning or neural networks, these methods may be challenging in a safety-critical environment. Black box methods often excel in contexts where exploration and failure are beneficial for training; however, failures in an industrial setting could risk the safety of people and equipment without proper safeguards.

7
Conclusions

The results show that the different controllers all have positive, and negative, aspects when used for discharging. It is possible to achieve safe temperature control, but often at the cost of computational complexity and requiring an accurate thermal model describing the system dynamics. It is encouraged for future work that the module-level modeling is expanded upon, and the capabilities of using one model for modules, based on different geometries, configurations, or chemistries, investigated.

CC-CV discharge is a simple control strategy, only relying on knowledge of the battery capacity and measurements of the terminal voltage and not necessarily a thermal model, unlike the other controllers used in this project. Depending on how the CV stage is implemented, the discharge could take a relatively long time to reach 0 % SoE, and especially the CV stage could take up the majority of the discharge time. This implies that increasing the current during the CC stage would not necessarily cause a significant decrease in discharge time but it could still cause a further rise in battery temperature, which could increase the risk of thermal runaway.

The CC-CT controller takes a middle-ground between controller complexity and safety. When estimating the core temperature, the results imply that there can be occurrences of oscillations around the setpoint which violates the set temperature constraint. This controller is dependent on the calibration of parameters beyond a thermal model of the battery. Depending on the parameters, the system can be prone to oscillations, or steady-state error, causing a drift in the setpoint tracking. This implies that during longer discharges, the battery temperature could increase above the setpoint, or lose optimality by dropping below the setpoint. Overshooting may occur if the proportional coefficient is set too high, while an excessively low value could result in a slow rise in temperature. This presents a trade-off between achieving a safe discharge temperature and potentially extending the discharge time. Lastly, it should be noted that the discharge current generated by the controller is not optimal in accordance with a cost function, but only a reaction to the system outputs to maintain a temperature setpoint.

The performance of the DP-generated current profile is highly dependent on the accuracy of the underlying prediction model. The results show that calculating the optimal discharge current offline could prove problematic, both regarding discharge time and avoiding constraint violations. If the model is inaccurate, it is possible to see a conservative profile, increasing the discharge time, or a profile that causes the temperature constraint to be violated for longer periods of time.

The MPC would be the recommended controller for this application if any are to be applied in a real-world scenario, based on its ability to maintain constraints and discharge time. The ability to utilize real-time data using a Kalman filter mitigates some of the reliance on an accurate prediction model, which could be useful for discharging different types of batteries other than that, or those, that are used when gathering data for the model. The controller could also be subjected to modifications, increasing robustness, such as the implementation of tube-based MPC in this project. It is, however, encouraged to consider using a non-linear model to better capture the battery dynamics, or investigating other models, more accurately describing the module-level dynamics, than was used in this project.

Bibliography

[1] IEA, "Global ev outlook," *IEA*, 2023. [Online]. Available: https://www.iea.org/reports/global-ev-outlook-2023.

[2] E. Sandberg, *Second life applications for de- graded ev batteries*, 2023.

[3] S. Kim, J. Bang, J. Yoo, *et al.*, "A comprehensive review on the pretreatment process in lithium-ion battery recycling," *Journal of Cleaner Production*, vol. 294, p. 126 329, 2021, ISSN: 0959-6526. DOI: https://doi.org/10.1016/j.jclepro.2021.126329. [Online]. Available: https://www.sciencedirect.com/science/article/pii/S0959652621005497.

[4] M. Shi, Y. Ren, J. Cao, Z. Kuang, X. Zhuo, and H. Xie, "Current situation and development prospects of discharge pretreatment during recycling of lithium-ion batteries: A review," *Batteries & Supercaps*, vol. 7, no. 2, e202300477, 2024. DOI: https://doi.org/10.1002/batt.202300477. eprint: https://chemistry-europe.onlinelibrary.wiley.com/doi/pdf/10.1002/batt.202300477. [Online]. Available: https://chemistry-europe.onlinelibrary.wiley.com/doi/abs/10.1002/batt.202300477.

[5] A. K. de Souza, G. Plett, and M. S. Trimboli, "Lithium-ion battery charging control using a coupled electro-thermal model and model predictive control," in *2020 IEEE Applied Power Electronics Conference and Exposition (APEC)*, 2020, pp. 3534–3539. DOI: 10.1109/APEC39645.2020.9124431.

[6] P. Lyu, X. Liu, J. Qu, *et al.*, "Recent advances of thermal safety of lithium ion battery for energy storage," *Energy Storage Materials*, vol. 31, pp. 195–220, 2020, ISSN: 2405-8297. DOI: https://doi.org/10.1016/j.ensm.2020.06.042. [Online]. Available: https://www.sciencedirect.com/science/article/pii/S2405829720302646.

[7] C. Zou, X. Hu, Z. Wei, and X. Tang, "Electrothermal dynamics-conscious lithium-ion battery cell-level charging management via state-monitored predictive control," *Energy*, vol. 141, pp. 250–259, 2017, ISSN: 0360-5442. DOI: https://doi.org/10.1016/j.energy.2017.09.048. [Online]. Available: https://www.sciencedirect.com/science/article/pii/S0360544217315712.

[8] Z. Wei, H. He, and J. Hu, "Unbiased model identification and state of energy estimation of lithium-ion battery," in *2020 IEEE Energy Conversion Congress and Exposition (ECCE)*, 2020, pp. 5595–5599. DOI: 10.1109/ECCE44975.2020.9235630.

[9] S. Gros, *Modelling and Simulation*. 2022, pp. 9–10.

[10] Z. Gajic, *Discrete-time systems: Chapter 8 lecture slides*, Accessed: 2024-10-04, 2024. [Online]. Available: http://eceweb1.rutgers.edu/~gajic/solmanual/slides/chapter8_DIS.pdf.

[11] A. Mondal, Y. Fu, W. Gao, and C. C. Mi, "Pretreatment of lithium ion batteries for safe recycling with high-temperature discharging approach," *Batteries*, vol. 10, no. 1, 2024, ISSN: 2313-0105. DOI: 10.3390/batteries10010037. [Online]. Available: https://www.mdpi.com/2313-0105/10/1/37.

[12] M. Sniedovich, "Dynamic programming and the principle of optimality: A systematic approach," *Advances in Water Resources*, vol. 1, no. 4, pp. 183–190, 1978, ISSN: 0309-1708. DOI: https://doi.org/10.1016/0309-1708(78)90001-5. [Online]. Available: https://www.sciencedirect.com/science/article/pii/0309170878900015.

[13] LG Energy Solution, *Cell Specifications*, Accessed: 2024-09-02, 2022. [Online]. Available: https://www.lgensol.com/assets/file/LGES_spec_sheet_cells_2022.pdf.

[14] PushEVs, *NCM 712 by LG Chem: E66A and E78 battery cells in detail*, Accessed: 2024-09-02, 2021. [Online]. Available: https://pushevs.com/2021/03/30/ncm-712-by-lg-chem-e66a-and-e78-battery-cells/.

[15] J. Löfberg, "Yalmip : A toolbox for modeling and optimization in matlab," in *In Proceedings of the CACSD Conference*, Taipei, Taiwan, 2004.

[16] A. Mosek, "The mosek optimization software," *Online at http://www. mosek. com*, vol. 54, no. 2-1, p. 5, 2010.

[17] E. C. D. E. N. A. Service, "Renewable energy storage from second-life batteries is viable but may benefit from subsidies," *European Commission*, 2023. [Online]. Available: https://environment.ec.europa.eu/news/renewable-energy-storage-second-life-batteries-viable-may-benefit-subsidies-2023-09-13_en.

[18] R. R. Richardson, S. Zhao, and D. A. Howey, "On-board monitoring of 2-d spatially-resolved temperatures in cylindrical lithium-ion batteries: Part i. low-order thermal modelling," *Journal of Power Sources*, vol. 326, pp. 377–388, 2016, ISSN: 0378-7753. DOI: https://doi.org/10.1016/j.jpowsour.2016.06.103. [Online]. Available: https://www.sciencedirect.com/science/article/pii/S0378775316308151.

DEPARTMENT OF SOME SUBJECT OR TECHNOLOGY
CHALMERS UNIVERSITY OF TECHNOLOGY
Gothenburg, Sweden
www.chalmers.se

CHALMERS
UNIVERSITY OF TECHNOLOGY